Journal of Controlled Release 172 (2013) 77–85

Contents lists available at SciVerse ScienceDirect

Journal of Controlled Release

journal homepage: www.elsevier.com/locate/jconrel

NANOMEDICINE

PEGylation of HPMA-based block copolymers enhances tumor accumulation *in vivo*: A quantitative study using radiolabeling and positron emission tomography

Mareli Allmeroth [a,1], Dorothea Moderegger [b,1], Daniel Gündel [d], Hans-Georg Buchholz [c], Nicole Mohr [a], Kaloian Koynov [e], Frank Rösch [b,2], Oliver Thews [d,3], Rudolf Zentel [a,*]

[a] Institute of Organic Chemistry, Johannes Gutenberg University, Duesbergweg 10–14, 55099 Mainz, Germany
[b] Institute of Nuclear Chemistry, Johannes Gutenberg University, Fritz-Strassmann-Weg 2, 55128 Mainz, Germany
[c] Department of Nuclear Medicine, University Medicine Mainz, Langenbeckstraße 1, 55131 Mainz, Germany
[d] Institute of Physiology, University Halle, Magdeburger Str. 6, 06097 Halle (Saale), Germany
[e] Max-Planck-Institute for Polymer Research, Ackermannweg 10, D-55128 Mainz, Germany

ARTICLE INFO

Article history:
Received 23 April 2013
Accepted 25 July 2013
Available online 14 August 2013

Keywords:
Fluorine-18 labeling
HPMA
PEG
PET
Structure–property relationships
Walker 256 mammary carcinoma

ABSTRACT

This paper reports the body distribution of block copolymers (made by controlled radical polymerization) with *N*-(2-hydroxypropyl)methacrylamide (HPMA) as hydrophilic block and lauryl methacrylate (LMA) as hydrophobic block. They form micellar aggregates in aqueous solution. For this study the hydrophilic/hydrophobic balance was varied by incorporation of differing amounts of poly(ethylene glycol) (PEG) side chains into the hydrophilic block, while keeping the degree of polymerization of both blocks constant. PEGylation reduced the size of the micellar aggregates (R_h = 113 to 38 nm) and led to a minimum size of 7% PEG side chains. Polymers were labeled with the positron emitter ^{18}F, which enables to monitor their biodistribution pattern for up to 4 h with high spatial resolution. These block copolymers were investigated in Sprague–Dawley rats bearing the Walker 256 mammary carcinoma *in vivo*. Organ/tumor uptake was quantified by *ex vivo* biodistribution as well as small animal positron emission tomography (PET).

All polymers showed renal clearance with time. Their uptake in liver and spleen decreased with size of the aggregates. This made PEGylated polymers – which form smaller aggregates – attractive as they show a higher blood pool concentration. Within the studied polymers, the block copolymer of 7% PEGylation exhibited the most favorable organ distribution pattern, showing highest blood-circulation level as well as lowest hepatic and splenic uptake. Most remarkably, the *in vivo* results revealed a continuous increase in tumor accumulation with PEGylation (independent of the blood pool concentration) — starting from lowest tumor uptake for the pure block copolymer to highest enrichment with 11% PEG side chains. These findings emphasize the need for reliable (non-invasive) *in vivo* techniques revealing overall polymer distribution and helping to identify drug carrier systems for efficient therapy.

1. Introduction

Over the last four decades "polymer therapeutics" have been intensively studied regarding their potential for drug delivery and especially in anticancer treatment [1]. Generally they offer the potential to change the body distribution of drugs. The key benefits of polymer based drug delivery systems are thus – compared to low molecular weight free drug – the reduction of toxic side effects in healthy tissue, an increase in plasma half-life compared to the pure chemotherapeutic agent and an enhanced accumulation in the tumor due to the enhanced permeability and retention (EPR) effect [2,3].

To be clinically applicable there are some essential requirements that need to be fulfilled by a polymer. Besides being non-toxic, non-immunogenic, and biodegradable – or respectively biocompatible with an adequate molecular weight to allow body elimination – the carrier system should protect the drugs (or other active compounds) *versus* degrading enzymes or fast uptake by the mononuclear phagocyte system (MPS) which would cause their rapid elimination from the blood stream. Considering these demands, PEGylation has become firmly established to prolong the pharmacokinetic properties of nanocarrier systems [4–9]. Its so-called "stealth properties" – responsible for low immunogenicity and antigenicity of the coated material – minimize the identification by opsonin proteins and thus the phagocytic uptake

* Corresponding author. Tel.: +49 6131 39 20361.
E-mail addresses: frank.roesch@uni-mainz.de (F. Rösch), oliver.thews@medizin.uni-halle.de (O. Thews), zentel@uni-mainz.de (R. Zentel).
[1] Both authors contributed equally.
[2] Tel.: +49 6131 39 25302.
[3] Tel.: +49 345 557 4048.

0168-3659/$ – see front matter © 2013 Published by Elsevier B.V.
http://dx.doi.org/10.1016/j.jconrel.2013.07.027

[5,10,11]. PEG has, however, the disadvantage of only possessing two endgroups for functionalization, whereas it is often desirable to work with multifunctional polymer systems which allow the linkage of drugs, different targeting groups and labels (*e.g.* fluorescent dyes). In this regard, poly(HPMA) is holding favorable characteristics. It has comparable biocompatibility and has already been validated by diverse preclinical and clinical studies [12–18]. In addition, it is multifunctional and can also be easily modified with hydrophobic groups to form micellar aggregates.

Previous studies on ^{18}F-radiolabeled HPMA homopolymers and random copolymers already revealed that the ratio of hydrophilicity/hydrophobicity as well as aggregate formation possessed a major impact on the body distribution in the living animal and improved pharmacokinetic characteristics could be achieved for a high molecular weight HPMA based random copolymer [19]. However, the superstructures/aggregates formed from hydrophilic/hydrophobic random copolymers are not well defined and highly dynamic [20]. Thus a controlled release of their payload at the targeting site cannot be guaranteed *in vivo*. In this regard, amphiphilic block copolymers have some major benefits. Their chemical structure is better defined and they possess a more defined core-shell structure in aqueous media. The hydrophilic exterior provides steric stabilization/shielding and the hydrophobic core enables the facile entrapment of lipophilic drugs [21]. As a result it could be shown that the unspecific cell uptake is much smaller for block copolymers than for random copolymers [22]. In addition aggregate formation is occurring rapidly due to their comparatively low critical micelle concentration (CMC) [22] and hence fast renal elimination can be diminished. All of these aspects underline the potential of block copolymer micelles as candidates for drug delivery [23,24].

Concerning their synthetic preparation, controlled radical polymerization techniques like atom transfer radical polymerization (ATRP) or reversible addition–fragmentation chain transfer RAFT [25–28] are promising routes to narrowly distributed polymer structures, especially in combination with reactive ester chemistry [22,29–31] RAFT offers an elegant access to a variety of polymer architectures and functional groups. Not only imaging moieties or therapeutics can be attached, the polymer nature of the hydrophilic shell can be easily modified, too.

Former studies in our group already demonstrated the successful synthesis of HPMA based block copolymers (with lauryl methacrylate as hydrophobic block) by means of the RAFT process [22,31]. Ongoing experiments in two different tumor models *in vivo* revealed – however – an enhanced uptake of the block copolymers by liver and spleen compared to random copolymers [32]. Thus only marginal amounts of the polymers could be detected in the tumor tissue. These findings are most likely attributed to the hydrodynamic radii of the investigated block copolymer structures (R_h > 100 nm) [22] which are much larger compared to random copolymers. This might lead to a direct filtration by the macrophages of the MPS. Based on these results, the reduction in aggregate size is a major demand to improve the biodistribution profile of the block copolymers. Hence increasing the hydrophilicity of the hydrophilic HPMA block by incorporation of highly hydrophilic PEG segments is a promising concept to decrease aggregate size by increasing steric stabilization. In addition PEG is known for its shielding efficacy towards opsonin proteins [5,10,11].

To investigate the impact of functionalization with poly(ethylene glycol) on the pharmacokinetic profile of HPMA based block copolymers, radiolabeling in combination with positron emission tomography is a helpful diagnostic tool. Until now, studies concerning the *in vivo* behavior of diverse HPMA and PEG based nanoparticles have been almost exclusively carried out using either γ-imaging radionuclides such as ^{99m}Tc, ^{111}In or $^{125/131}$I [33–37] providing relatively low spatial resolution or by means of the metallic positron emitter ^{64}Cu which requires chelating agents [38–41]. In contrast to these approaches, we demonstrated the successful radiolabeling of various HPMA based polymers with the positron emitters $^{72/74}$As [42] and ^{18}F [43], thereby establishing PET imaging to assess the *in vivo* capability of potential drug delivery systems. Notably the shorter-lived ^{18}F ($t_{1/2}$ = 110 min) – combining ideal nuclear characteristics for high resolution PET imaging and upon labeling not influencing the polymer structure – can serve as useful tool to screen potential drug delivery systems based on their initial distribution and excretion pattern. It allows monitoring the distribution of the polymers for up to 5 h after administration. This time frame is too short to prove the EPR-effect. It allows one, however, to determine the general suitability of different polymer structures regarding excretion, MPS uptake, blood concentration and tumor uptake. Hence, short-term PET imaging can serve as a convenient tool to provide direct information on whether alterations of the polymer architecture are affecting the body distribution favorably (*e.g.* resulting in higher blood concentrations) or not (*e.g.* higher uptake in liver and spleen). These results are important for all types of drug delivery. With regard to the poly(HPMA) copolymers presented here, these results are especially important concerning the attempts to transport drugs over the blood–brain barrier [44,45].

In this work we have focused on minimizing aggregate size and protein interaction of new HPMA-*b*-LMA copolymers by incorporating different percentages of a linear, amine-functionalized $PEG_{2000\ Da}$ fragment into the hydrophilic block. This approach was aimed to optimize blood retention time by reducing the size of the micellar aggregates. In order to correlate the influence of PEG content on the resulting pharmacokinetics *in vivo*, the block copolymers were radiolabeled with the positron emitting nuclide ^{18}F. This enabled to investigate the influence of the molecular structure on the body distribution as well as tumor accumulation in the experimental Walker 256 mammary carcinoma model. In addition, the cellular uptake into tumor cells of PEGylated block copolymers was analyzed.

2. Material and methods

2.1. Materials

All solvents were of analytical grade, as obtained in Sigma-Aldrich and Acros Organics. Dioxane was distilled over a sodium/potassium composition, di-chloromethane over calcium hydride. Lauryl methacrylate was distilled to remove the stabilizer and stored at −18 °C. 2,2′-Azoisobutyronitrile (AIBN) was recrystallized from diethyl ether and stored at −18 °C as well.

2.2. Experimental setups

Experimental setups can be found in the Supplementary material.

2.3. Synthesis of the polymers $\mathbf{P_{0\%}}$ to $\mathbf{P_{11\%}}$

2.3.1. Synthesis of reactive ester homopolymer (macro-CTA)

RAFT polymerization of pentafluorophenyl methacrylate with 4-cyano-4-((thiobenzoyl)sulfanyl)pentanoic acid was carried out in a Schlenk tube [22,46]. For this purpose, 4 g of PFPMA was dissolved in 5 mL of absolute dioxane; furthermore CTP and AIBN were added. The molar ratio of CTP/AIBN was chosen as 1:8. After three freeze–vacuum–thaw cycles, the mixture was immersed in an oil bath at 65 °C and stirred over night. Afterwards, the polymeric solution was precipitated three times in hexane, centrifuged and dried under vacuum at 40 °C over night. A slightly pink powder was obtained. For ^{1}H NMR data see Supplementary material.

2.3.2. Synthesis of the reactive ester block copolymer

The macro-CTA obtained after homopolymerization of PFPMA was dissolved in dioxane; afterwards lauryl methacrylate as well as AIBN was added. As an example, 250 mg of macro initiator was dissolved in 5 mL dioxane, lauryl methacrylate and AIBN (1:8 ratio macro-CTA/AIBN) that were mixed. After three freeze–vacuum–thaw cycles, the mixture was immersed in an oil bath at 65 °C and stirred for three

days. Afterwards, poly(PFPMA)-*b*-poly(LMA) was precipitated three times in ethanol, centrifuged and dried under vacuum at 40 °C over night. A slightly pink powder was obtained. For ^{1}H NMR data see Supplementary material.

2.3.3. Removal of dithioester groups

The dithiobenzoate endgroup was removed using the protocol reported by Perrier et al. [47].

2.3.4. Synthesis of amine functionalized PEG_{2000} fragment

To synthesize the PEG_{2000}-amine fragment, a modified two step synthesis was accomplished [48]. For more details see the Supplementary material.

2.3.5. Polymer analogous reaction block copolymers

For radioactive labeling of block copolymers the protocol was applied as follows. 100 mg of poly(PFPMA)-*b*-poly(LMA) copolymer was dissolved in 2 mL of absolute dioxane. Exemplary for $\mathbf{P_{7\%}}$ (M_n = 25,000 g/mol), 5.4 mg of tyramine and 4 mg of triethylamine were diluted in a DMSO/dioxane mixture and added to the vessel. After stirring for 10 h at 45 °C, 160 mg of amine-functionalized $PEG_{2\ kDa}$ in 500 μL DMSO as well as 8 mg of triethylamine was added and the solution was stirred for 1 and 1/2 days. Thereafter, 21 mg of 2-hydroxypropylamine and 28 mg of Et_3N were added and the solution was further stirred for 48 h. For final removal of reactive ester side groups 20 mg of 2-hydroxypropylamine was additionally added the next morning. The solution was precipitated two times in diethyl ether, centrifuged and finally dissolved in a DMSO/water solution for dialysis. After lyophilization a white, crystalline powder could be obtained. For ^{1}H NMR data see Supplementary material. For additional fluorescent labeling, 100 mg of polymeric precursor was diluted in 2 mL of absolute dioxane and 2.9 mg of Oregon Green 488 cadaverine was added. Afterwards tyramine, PEG-$amine_{2\ kDa}$ and 2-hydroxypropylamine were added, as described by the procedure above.

2.4. Characterization of the polymers

The hydrodynamic radii of the polymeric systems were determined by Fluorescence Correlation Spectroscopy (FCS) using a commercial FCS setup. Thereby aggregate formation of the block copolymers can be proven. The details can be found in the Supplementary material.

2.5. Radiolabeling and purification for ex vivo and in vivo experiments

Radiolabeling and subsequent purification of the polymers for *ex vivo* and *in vivo* experiments were accomplished using an ^{18}F-fluoro-ethylation method modified from Herth et al. [43]. In brief, 3 mg of polymer was dried azeotropically three times each with 1 mL of acetonitrile prior to ^{18}F-fluorination. 100 μL of dry dimethylsulfoxide (DMSO) as well as 1 μL of 5 M Cs_2CO_3 solution was added and the labeling reaction was started by adding a dry solution of [^{18}F]fluoroethyl tosylate (FETos) in DMSO. Radiolabeling was performed at 120 °C for 18 min. Further details are given in the Supplementary material.

2.6. Animal experiments

We have not determined the cytotoxicity of the PEGylated copolymers. However the cytotoxicity of not-pegylated block copolymers analogous to $\mathbf{P_{0\%}}$ was tested [22]. It is above 0.1 mg/mL. For statistical copolymers no cytotoxicity was observed up to 1 mg/mL [45]. Based on the high biocompatibility of PEG, we do not expect that the PEGylated polymers posses a lower cytotoxicity limit.

2.6.1. Tumor and animal model

Cells lines were grown in culture in RPMI medium supplemented with 10 mM L-glutamine and 10% fetal calf serum (FCS) at 37 °C under a humidified 5% CO_2 atmosphere and sub-cultivated twice per week. For tumor implantation male Sprague–Dawley rats (Charles River Wiga, Sulzfeld, Germany; body weight 195 to 315 g) housed in the animal care facility of the University of Mainz were used in this study. All experiments had previously been approved by the regional animal ethics committee and were conducted in accordance with the German Law for Animal Protection and the UKCCCR Guidelines [49].

Animals were allowed access to food and acidified water *ad libitum* before the investigations. Solid carcinomas were heterotopically induced by injection of cell suspension (0.4 mL approx. 10^4 cells/μL) subcutaneously into the dorsum of the hind foot. Tumors grew as flat, spherical segments and replaced the subcutis and corium completely. Volumes were determined by measuring the three orthogonal diameters (d) of the tumors and using an ellipsoid approximation with the formula: $V = d_1 \times d_2 \times d_3 \times \pi / 6$. Tumors were used when they reached a volume of between 0.5 and 3.0 mL approx. 7 to 14 days after tumor cell inoculation.

2.6.2. In vivo μPET imaging

The μPET imaging was performed on a microPET Focus 120 small animal PET (Siemens/Concorde, Knoxville, USA). Animals were placed supine and breathed room air spontaneously. Dynamic PET studies were acquired in list mode. The radiolabeled polymers were administered as a bolus injection of 0.4–0.7 mL simultaneously with the start of the PET scan. The mean injected activity of labeled polymers was 21.7 ± 2.2 MBq. The PET list mode data were histogrammed into 25 frames and reconstructed using OSEM2D algorithm. Volumes-of-interests (VOIs) were defined for tumor and reference tissues (testis). The testis was used as a reference since it was in the field of view when imaging the tumors on the feet and because the tissue concentration was relatively constant between all animals on a low level. Time activity curves (TACs) were obtained with varying time frames (1.5–10 min) for a total measuring interval of 120 min. Ratios of tumor to reference tissue were calculated from integral images between 15′ and 120′ after polymer injection.

2.6.3. Biodistribution and cellular uptake studies

In order to assess the distribution of the radiolabeled polymers in different organs of the animals, the polymer (concentration of 1 mg in 1 mL sodium chloride solution) was injected i.v. in anesthetized tumor-bearing rats *via* the tail vein with a mean activity of 11.1 ± 0.4 MBq. After 120 or 240 min, the animals were sacrificed and different organ (kidney, liver, lung, spleen, heart, skeletal muscle, small intestine, testis, blood) and tumor samples were taken. The tissue samples were weighed and minced. Finally, the ^{18}F-activity in the organs was measured in a γ-counter.

Cellular studies can be found in the Supplementary material.

2.6.4. Statistical analysis

Results are expressed as means ± SEM. Differences between groups were assessed by the two-tailed Wilcoxon or Kruskal–Wallis test for unpaired samples. The significance level was set at $\alpha = 5\%$ for all comparisons. Correlation analysis was performed by calculating the Pearson's correlation coefficient.

3. Results and discussion

3.1. Synthesis and radioactive labeling of HPMA-b-LMA copolymers with varying $PEG_{2000\ Da}$ contents

This study focuses on the reduction of aggregate size of HPMA-*b*-LMA copolymers by covalently attaching different ratios of $PEG_{2000\ Da}$ segments to the hydrophilic block. The internal structure of the aggregates formed by the parent block copolymers in water is not known [22,31]. However their size (hydrodynamic radius R_h of about 100 nm) is far too large to result from simple micellar structures, because in this

case they could not be much larger than the individual polymer chains (expected R_h some nm). So either the shielding of the hydrophobic cores is insufficient or there may be some interactions among the hydrophilic corona. Based on these facts it seems reasonable to introduce some PEG chains into the hydrophilic corona to increase its hydrophilicity (the hydrophilicity of PEG – as determined from the second viral coefficient in aqueous solutions – is about a factor of ten larger than that of poly(HPMA) (second viral coefficient in water of poly(HPMA)): $2.6 * 10^{-4}$ mL g^{-2} mol [50]; of PEG ($M_n > 1.000$ g/mol): $3 * 10^{-3}$ mL g^{-2} mol [51]) and thereby to decrease the size of the aggregates. In addition PEG is only an acceptor for H-bonding whereas poly(HPMA) is both a donor and an acceptor. Thus it can be assumed that the incorporation of PEG will reduce the interaction among the hydrophilic corona. A further advantage of incorporating some PEG units into the hydrophilic parts can result from the stealth effect of PEG and its minimal tendency for interaction with opsonin proteins [5,10,11,52].

For a comparison of the different block copolymers it is essential that they all have the same degree of polymerization. This can be achieved by the synthetic preparation route used. Due to the reactive ester approach, PEG chains can be easily grafted to the polymeric backbone within the hydrophilic block and thus different degrees of PEGylation can be realized starting from the same precursor block copolymer. Consequently all polymers have the same number of repeating units and the degree of polymerization $\mathbf{P_n}$ – both in the hydrophilic and in the hydrophobic blocks – is independent of the degree of functionalization with short PEG chains.

Overall, five different block copolymer structures were synthesized ($\mathbf{P_{0\%}}$ to $\mathbf{P_{11\%}}$), starting from the same reactive block copolymer precursor system (**P*–R**). A reaction scheme of the polymer synthesis is illustrated in Fig. 1. The polymer characteristics are summarized in Table 1.

Starting from the reactive ester monomer pentafluorophenyl methacrylate (PFPMA) the macro-chain transfer agent (macro-CTA) was synthesized and further converted to reactive ester block copolymer **P*–R**. By polymer analogous reaction of the reactive ester block, tyramine groups (incorporation of ~3%) for radiolabel attachment as well as the amine-functionalized PEG_{2000} fragment and 2-hydroxypropylamine were covalently linked to form the hydrophilic block. Thus both the hydrophilic and the hydrophobic blocks of all block copolymers have the same degree of polymerization $\mathbf{P_n}$. For FCS measurements and studies of cellular uptake, a fluorescently labeled version of all block copolymers was prepared in addition (labeled with 1 mol% of Oregon Green, structure not shown).

To perform non-invasive small animal PET imaging as well as for quantification by *ex vivo* biodistribution measurements, the positron emitter fluorine-18 was introduced *via* [^{18}F]fluoroethylation, a method already established for various HPMA based copolymers [19,43]. In order to promote the incorporation of the fluoroethyl radiolabel, the previously applied radiolabeling conditions [43] were adjusted by using Cs_2CO_3 as base as well as azeotropic drying of the polymer precursors prior to radiolabeling. Nevertheless, radiolabeling efficiencies – as listed in Table 1 – were still comparably low, with highest radiochemical yields (RCYs) achieved for block copolymer $\mathbf{P_{11\%}}$ (RCY = 18 ± 2%).

As shown in Table 1, well-defined and narrowly distributed block copolymer systems could be synthesized (polydispersity index = 1.25) as determined by GPC for **P*–R**. The hydrophobic lauryl methacrylate segment was incorporated in a ratio of 25% as determined by ^{1}H NMR spectroscopy. PEG_{2000} segments were linked to the hydrophilic block with amounts of 1, 5, 7 and 11 mol% as determined by ^{1}H NMR spectroscopy. This leads to an increase of the (calculated) molecular weight (M_w) of the final polymer structures from 21,000 to 47,000 g/mol and a

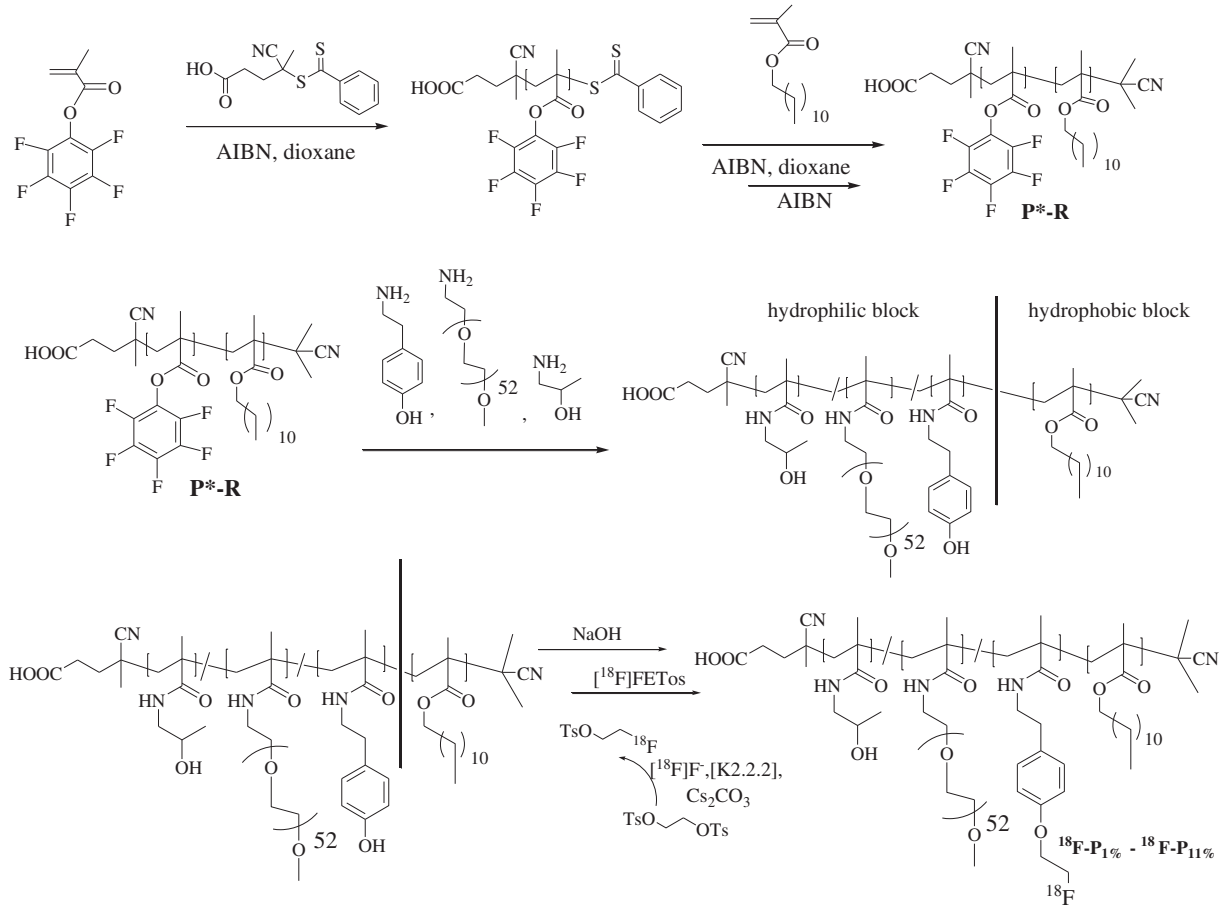

Fig. 1. Polymer synthesis as well as radioactive labeling procedure (exemplified for PEG_{2000} modified polymers). For characterization see Table 1. For FCS measurements the polymers were additionally modified with 1 mol% of Oregon Green.

Table 1
Analytical data of reactive ester precursor polymer (**P*–R**) and final block copolymer structures (**$P_{0\%}$** to **$P_{11\%}$**).

Nomenclature	Polymer structure	Ratio of block length	PEG_{2000} incorp.[4]	M_n in g/mol	M_w in g/mol	R_h[5] in nm	RCY in %
P*–R	Block copolymer	–	–	25,000[1]	31,000[1]	n.d.	n.d.
$P_{0\%}$	Block copolymer	75:25%[2]	0%	17,000[3]	21,000[3]	112.8 ± 5.7	7 ± 0
$P_{1\%}$	Block copolymer	75:25%[2]	1%	20,000[3]	24,000[3]	55.4 ± 2.9	11 ± 1
$P_{5\%}$	Block copolymer	75:25%[2]	5%	26,000[3]	33,000[3]	38.0 ± 2.1	15 ± 8
$P_{7\%}$	Block copolymer	75:25%[2]	7%	30,000[3]	38,000[3]	38.1 ± 2.1	5 ± 1
$P_{11\%}$	Block copolymer	75:25%[2]	11%	39,000[3]	47,000[3]	53.0 ± 2.8	18 ± 2

[1] = Determination by gel permeation chromatography (GPC) in THF as solvent; [2] = Monomer ratio determined by ^{1}H NMR spectroscopy after polymer analogous reaction with 2-hydroxypropylamine for polymer **$P_{0\%}$**; [3] = Calculated from the molecular weight of the reactive ester polymer **P*–R** as determined by GPC in THF as solvent; [4] = PEG_{2000} incorporation (incorp.) ratio determined by ^{1}H NMR spectroscopy after polymer analogous reaction; [5] = Hydrodynamic radii of the aggregates determined by Fluorescence Correlation Spectroscopy (FCS) in aqueous NaCl solution, concentration: 0.1 mg/mL; RCY = radiochemical yield.

corresponding increase of R_h of the individually dissolved polymers (unimers) in DMSO (good solvent) from 4.6 nm to 5.2–5.6 nm as determined by fluorescence correlation spectroscopy (see Supplementary material). In water the size of the unimers is strongly reduced (about 1.6 nm for all block copolymers) presumably because of the collapse of the hydrophobic block. GPC measurements (see Supplementary material) show about the same polydispersity (1.2 to 1.4) for the unimers of all block copolymers.

In order to probe the aggregation behavior of the block copolymers and estimate their CMC we have performed FCS experiments in aqueous (0.9% isotonic NaCl) solutions with increasing polymer concentrations (see Supplementary material) for block copolymers **$P_{0\%}$**, **$P_{5\%}$** and **$P_{11\%}$**. At a very low concentration almost no aggregates were detected for all three polymers. Aggregation starts at a concentration of 10^{-4} mg/mL for all polymers, irrespective of the degree of PEGylation. Thus there is only a minor and non-systematic influence of PEGylation on the CMC which stays between 10^{-5} and 10^{-4} mg/mL^{-1}. However PEGylation reduces the size of the aggregates (see Supplementary material). The pure HPMA–LMA block copolymer **$P_{0\%}$** exhibited a hydrodynamic radius R_h of 112.8 nm, thereby representing the largest aggregate structure investigated in this study. As expected the incorporation of PEG chains into the HPMA corona reduces the R_h values of the block copolymer aggregates and leads to a minimum for **$P_{5\%}$** and **$P_{7\%}$** (~38 nm) despite the increase of the size of the individual polymers (unimers). This result stays in good correlation with earlier studies on PEG-coated nanoparticles by Gref et al. [53]. However polymer **$P_{11\%}$** – incorporating 11% PEG segments – shows again an increase of the hydrodynamic radius of the aggregates to 53 nm. Generally the size of all aggregates/micellar superstructures found is far too large to be explained by a simple polymer micelle because in this case they could not be much larger than the individual polymer chains. Obviously compound micelles with a more complex inner structure are formed, in which several hydrophobic cores are interconnected somehow. These aggregates are in equilibrium with free polymer chains (unimers) as proven by FCS measurements (see Supplementary material).

3.2. Organ distribution

As it is known that both PEG length and surface density of the hydrophilic block hold a tremendous impact on clearance from the bloodstream [39,41,54], herein block copolymers with varying PEG_{2000} contents (0–11% incorporation) were investigated.

Quantification of the recovered dose of radiofluorinated block copolymers was accomplished in selected organs (liver, spleen, kidney, heart, blood, lung, muscle, small intestine and testis) 2 h and 4 h after i.v. administration.

The resulting biodistribution data of polymers with different degrees of PEGylation in the organs is illustrated in Fig. 2 and Table 2 (4 h values are presented in Table S4; see Supplementary material).

Liver accumulation of **$P_{0\%}$** to **$P_{11\%}$** over a time frame of 4 h can be seen in Fig. 2A. Highest hepatic uptake was determined for polymers with lowest degree of PEGylation (**$P_{0\%}$** = 5.27 ± 0.35 and **$P_{1\%}$** = 6.24 ± 0.11% ID/g tissue after 4 h p.i.). In contrast, **$P_{7\%}$** was the polymer with lowest levels in the liver; only 2.47 ± 0.06% ID/g tissue was detected after 4 h. However the even further pegylated polymer **$P_{11\%}$** showed again an increase in liver accumulation, presumably as a consequence of the size increase of the aggregates. A quite comparable trend can be observed in the spleen (Fig. 2B). The pure block copolymer **$P_{0\%}$** showed highest splenic uptake over time (4.84 ± 1.30% ID/g tissue 4 h p.i.) whereas the polymer with 7% of PEGylation **$P_{7\%}$** was accumulating to the lowest extent (1.64 ± 0.07% ID/g tissue 4 h p.i.). Liver and spleen uptake decreases – over all – with decreasing size of the aggregates. It should be noted in this context that a HPMA-based random copolymer (**P4*** from Ref. [19]) which formed aggregates of about the same size (R_h: 40 nm) as **$P_{7\%}$** showed a comparable low uptake in liver and spleen and thus a high concentration in the blood pool.

Fig. 2C is showing the overall renal uptake of the PEG_{2000}-modified HPMA–LMA block copolymer systems. Highest renal filtration could be seen for **$P_{0\%}$**, further increasing over time (7.95 ± 0.96 to 9.45 ± 1.12% ID/g tissue after 4 h). For comparison it should, however, be noted that this value is smaller than the one of a homopolymer [19] of a very high molecular weight (M_w: 55 kDa). So aggregate formation in block copolymers hinders excretion through the kidneys but the extent depends on aggregate and molecular structure. With rising PEG level, kidney uptake was diminished — with a minimum for **$P_{7\%}$**. Overall all polymeric systems showed renal clearance over time as proven by the fact that the polymers were also detected in the bladder (see Fig. 4). In addition polymer excretion was measured in the urine. However, due to spontaneous urination during the observation period the exact determination of the excreted amount of polymers was not feasible and in some animals no urine could be collected. The excreted polymer was 1.72–2.16% of the injected dose per gram urine for all PEGylated polymers whereas the amount of the non-PEGylated polymer was about 1.36%/g urine. These data confirm that all polymers were excreted by the kidney to a similar extent. A different trend was observed regarding blood pool concentrations of the varying polymer systems (Fig. 2D). Lowest blood circulation times were detected for **$P_{0\%}$** and **$P_{1\%}$**, the polymers with lowest PEG contents (0.45 ± 0.05 and 0.26 ± 0.01% ID/g tissue 4 h p.i.). An augmentation in PEGylation resulted in an almost linear increase of polymer concentration in the blood. A nearly 5-fold higher blood pool concentration of **$P_{7\%}$** compared to the non-PEGylated block copolymer **$P_{0\%}$** could be seen after 2 h. Concerning the positive influence of PEG there seems to be a limit of PEGylation efficacy as demonstrated for decreasing blood concentration of block copolymer **$P_{11\%}$** (0.90 ± 0.02% ID/g tissue after 4 h). In general, blood levels of all polymers decreased over the prolonged observation time of 4 h (Fig. 2D) indicating the ongoing excretion of the polymers, presumably by the kidney (Fig. 2C). Thus the system with the lowest uptake by liver, spleen and kidney shows the highest concentration in the blood pool. Highly blood supplied organs such as the heart and lung directly reflect the blood concentration pattern — exhibiting a minimum level of block copolymer **$P_{1\%}$** and highest values for **$P_{7\%}$** (see Table 2 and Fig. S1/Table S3 Supplementary material). In addition to these findings, polymer accumulation in muscle, small intestine and testis was comparatively low,

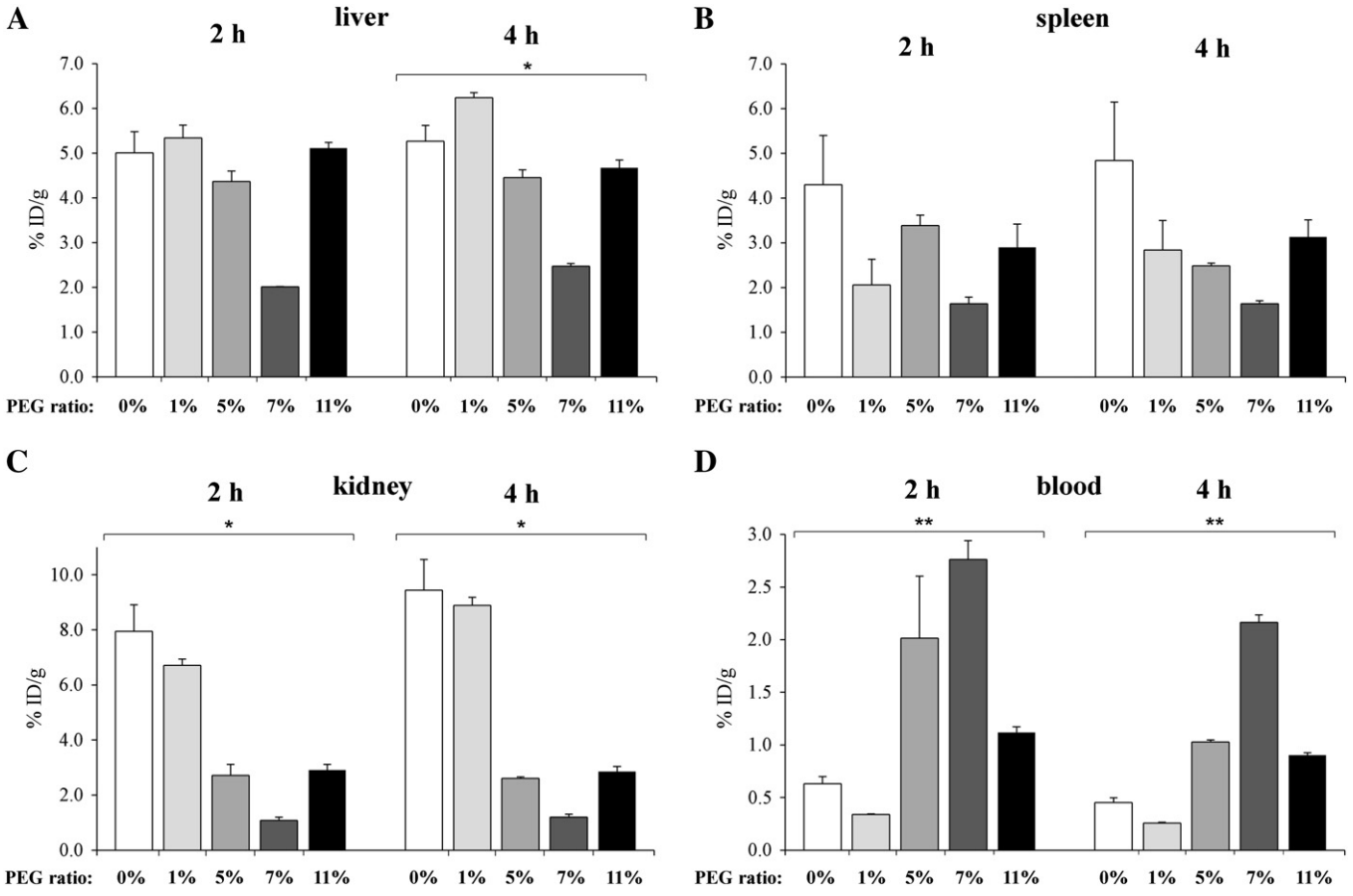

Fig. 2. Biodistribution of polymer structures $\mathbf{P_{0\%}}$ to $\mathbf{P_{11\%}}$, in selected organs (kidney, liver, spleen and blood) 2 and 4 h p.i. (0% n = 6, 1% n = 3, 5% n = 3, 7% n = 2, 11% n = 3); (*) $p < 0.05$, (**) $p < 0.01$.

not demonstrating great differences between the five examined block copolymers varying in PEG_{2000} incorporation efficiencies (*cf.* Tables 2 and S3 Supplementary material).

In regard to these results some major conclusions can be drawn. Overall, the uptake of polymers in the spleen (and also the liver) seems to correlate with the size of their aggregates (hydrodynamic radii in Table 1), although this correlation is not very strict as $\mathbf{P_{5\%}}$ and $\mathbf{P_{7\%}}$ exhibit a comparable R_h of 38 nm but demonstrate different liver and spleen accumulation patterns *in vivo*. Nevertheless, a smaller aggregate size combined with a medium degree of PEGylation seems to be beneficial for a reduced recognition by the MPS and thus a decreased hepatic uptake — as particularly seen for $\mathbf{P_{7\%}}$. These results support our concept to introduce poly(ethylene glycol) side chains into block copolymers to reduce the size of their micellar aggregates and avoid fast clearance by the mononuclear phagocyte system.

Table 2
Polymer uptake in different organs expressed by the fraction of the injected dose (ID) of the polymer per gram tissue 2 h after i.v. injection (0% n = 6, 1% n = 3, 5% n = 3, 7% n = 2, 11% n = 3).

	Polymer concentration [% ID/g tissue]				
Organ	0% PEG	1% PEG	5% PEG	7% PEG	11% PEG
Lung	0.39 ± 0.06	0.23 ± 0.01	0.74 ± 0.18	1.15 ± 0.01	0.89 ± 0.26
Liver	5.01 ± 0.47	5.34 ± 0.29	4.37 ± 0.23	2.01 ± 0.01	5.11 ± 0.13
Spleen	4.30 ± 1.10	2.06 ± 0.57	3.39 ± 0.51	1.64 ± 0.15	2.90 ± 0.52
Kidney	7.95 ± 0.96	6.72 ± 0.22	2.71 ± 0.41	1.09 ± 0.11	2.91 ± 0.20
Muscle	0.07 ± 0.01	0.04 ± 0.01	0.10 ± 0.03	0.05 ± 0.01	0.07 ± 0.01
Heart	0.22 ± 0.03	0.11 ± 0.01	0.39 ± 0.08	0.61 ± 0.01	0.31 ± 0.03
Blood	0.63 ± 0.07	0.34 ± 0.01	2.01 ± 0.59	2.76 ± 0.18	1.12 ± 0.05
Small intestine	0.23 ± 0.02	0.14 ± 0.01	0.22 ± 0.02	0.25 ± 0.05	0.31 ± 0.06
Testis	0.10 ± 0.01	0.07 ± 0.01	0.19 ± 0.03	0.19 ± 0.01	0.17 ± 0.01

In terms of renal filtration it has to be mentioned that all investigated polymer structures (R_h varying from 38 to 113 nm) are far too big for being filtered by the kidneys (renal threshold limit of 5–6 nm in diameter [55]). Since all polymers still demonstrate renal filtration, the balance between unimers (diameter in aqueous solution below 4 nm ($2 * R_h$), see Supplementary material) and micellar superstructures must be the major factor responsible for the observed *in vivo* characteristics. For all block copolymers compared here the CMC is in a comparable range (below 10^{-4} mg/mL). But little is known about how the equilibrium between unimers (individual polymer chains) and the micellar aggregates may be shifted in the basal membrane of the kidney. Increasing the amount of PEG chains in the hydrophilic block might also protect the aggregates from interactions with the highly charged basal membrane of the kidney and thereby protect them. In addition it has to be considered that the size of the unimers increases with increasing PEG content. Thus it gets more complicated for them to pass the kidney.

Blood pool concentrations of the different block copolymer structures are the direct result of their uptake/filtration in liver, spleen and kidney. Polymers with lowest levels in the excretion organs – particularly $\mathbf{P_{5\%}}$ and $\mathbf{P_{7\%}}$ – are demonstrating highest blood residence time. In general PEGylation is explicitly improving the plasma half-life of the herein investigated polymer structures thus staying in good agreement with studies of Torchilin et al. on the impact of PEGylation on liposomes in mice [56].

3.3. Tumor accumulation

For analysis of the polymer uptake *in vivo* Walker 256 mammary carcinomas were used with a volume of 1.46 ± 0.16 mL. Quantitative biodistribution studies of the tumor tissue were accomplished 2 and 4 h post-injection of the polymer compounds. This time span is too short to

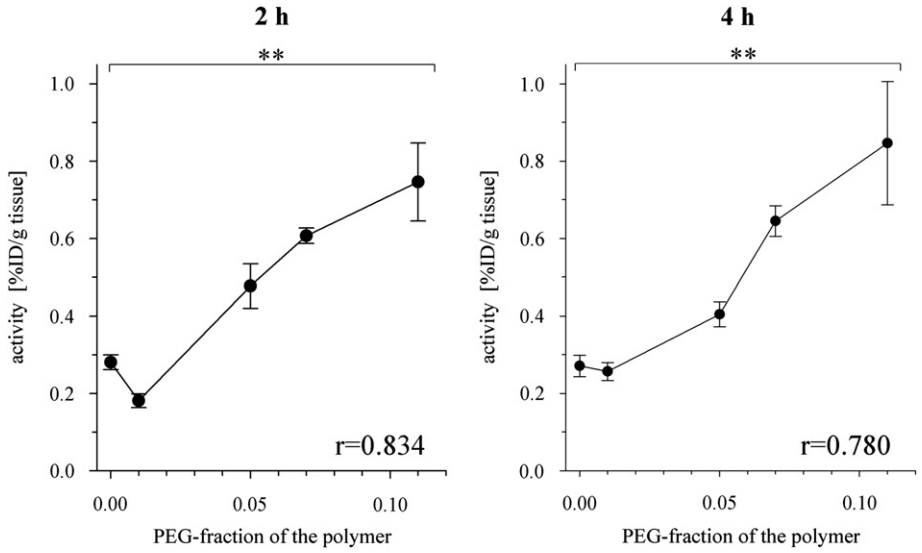

Fig. 3. Tumor accumulation of polymers as a function of the incorporated amount of PEG_{2000} (n = 6 for 0%, 1%, 5% and 11% PEG; n = 4 for 7% PEG); (**) $p < 0.01$.

prove the EPR-effect. But it is perfectly suited to study, if the tumor is well reached depending on molecular structure and aggregate formation. The dependency of PEGylation on the % ID/g tumor is depicted in Fig. 3.

As clearly seen HPMA–LMA copolymers with lowest degree of PEGylation – $\mathbf{P_{0\%}}$ and $\mathbf{P_{1\%}}$ – also showed lowest accumulation in the tumor tissue. Starting from the above mentioned polymer structures tumor enrichment increases continuously with increasing PEGylation being highest for $\mathbf{P_{11\%}}$, the polymer with highest PEG content. In all cases the concentration in the tumor increases from 2 to 4 h, although the blood pool concentration decreases from 2 to 4 h (Fig. 2). Based on these results, a direct correlation between PEG_{2000} incorporation ratio and tumor uptake can be drawn. The higher the PEGylation efficacy of the polymer structures, the higher the tumor uptake over the observed time frame. Furthermore it has to be noted that $\mathbf{P_{11\%}}$ showed highest tumor enrichment after 4 h even though its blood levels were distinctly lower compared to $\mathbf{P_{7\%}}$. This observation is demonstrating that tumor accumulation is not solely affected by the retention of the polymers in the circulation. Besides $\mathbf{P_{11\%}}$ exhibited a higher hydrodynamic radius (53 nm) compared to $\mathbf{P_{7\%}}$ (38 nm), being of potential importance regarding its residence time in the tumor tissue.

3.4. MicroPET imaging and cellular uptake studies

Besides quantification of organ accumulation – clearly demonstrating a correlation of PEGylation on organ distribution and tumor uptake *ex vivo* – both static and dynamic μPET studies were accomplished in Walker 256 carcinoma bearing rats. Whole-body μPET images (Fig. 4), acquired 2 h post injection, stay in good accordance to the distribution data obtained in major organs (Fig. 2). PET images reveal kidney and bladder accumulation for all block copolymers hence confirming renal clearance. Furthermore, PET studies clearly displayed the disparities regarding blood circulation lifetimes according to different degrees of PEG incorporation. Whereas neither heart nor aorta is displayed in case of $\mathbf{P_{0\%}}$ and $\mathbf{P_{1\%}}$, PET images of block copolymers exhibiting higher PEG content ($\mathbf{P_{5\%}}$, $\mathbf{P_{7\%}}$, $\mathbf{P_{11\%}}$) explicitly show remaining activity in the blood compartment. This observation is illustrating the enhanced circulation of PEGylated block copolymers in the blood pool which is essential for effective drug delivery (in correspondence with the *ex vivo* biodistribution data, Fig. 2).

In addition the uptake of PEG modified block copolymers in the Walker 256 carcinoma was studied using dynamic μPET imaging over

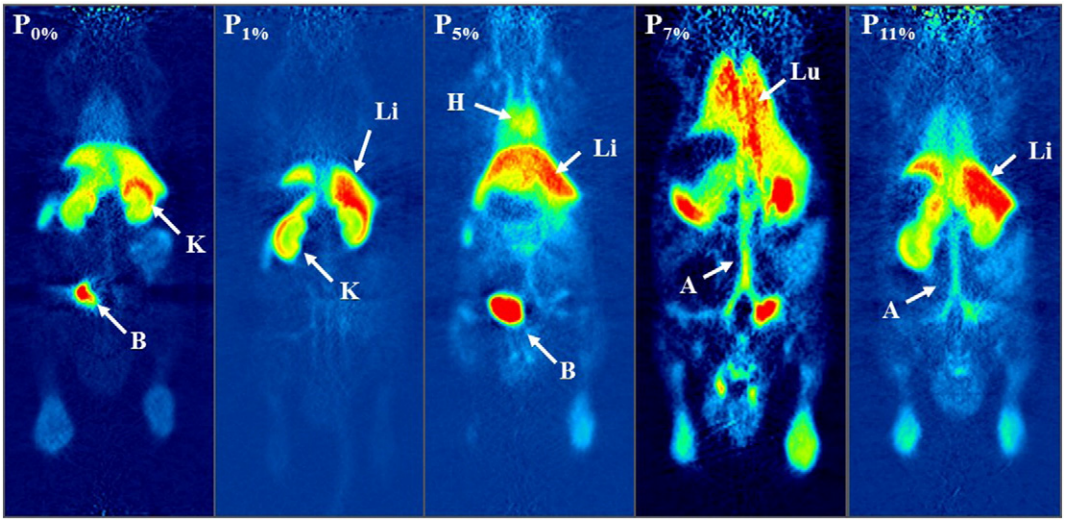

Fig. 4. Whole body μPET image sections obtained 120–135 min after administration of ^{18}F-polymers showing renal clearance (kidney (K), bladder (B)), distribution in liver (Li) and lung (Lu) as well as enhanced blood retention (heart (H), aorta (A)) of PEGylated polymers.

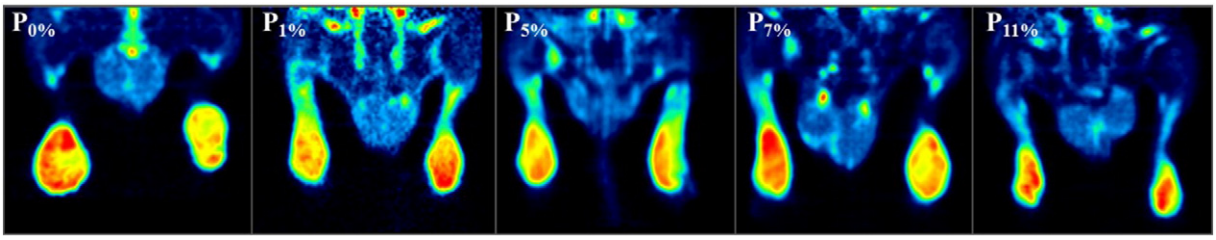

Fig. 5. Examples of coronal μPET image sections of Walker 256 tumors 60–120 min after i.v. administration of polymers with varying PEG contents illustrating tumor accumulation.

the course of 2 h after i.v. injection. Coronal slices of summed μPET images through the tumors – implanted at the hind foot dorsum – (Fig. 5) clearly display polymer uptake for all ^{18}F-labeled polymers.

Finally the question arises on how the disparities in tumor accumulation (see Fig. 3) and blood pool retention (Fig. 2) can be explained. Now besides blood pool concentration, also diffusion into the tumor tissue and uptake in the tumor cells are essential. As the PEGylated block copolymers **P$_{1\%}$** to **P$_{11\%}$** all show a comparable size of the aggregates the cellular uptake seemed most important. Thus we additionally investigated the cellular uptake into Walker 256 cells *in vitro*. Fig. 6 indicates pronounced differences between the block polymers. Cellular uptake was highest for non- and low PEGylated polymers (**P$_{0\%}$** and **P$_{1\%}$**) whereas the highly PEGylated compounds **P$_{5\%}$** to **P$_{7\%}$** showed a lower intracellular accumulation. This is according to expectations as PEGylation – in general – renders polymers more "stealth-like" and reduces cellular uptake. But astonishingly the most pegylated polymer **P$_{11\%}$** showed again a higher cellular uptake. This observation, even if not well understood, explains the discrepancy between blood pool concentration (Fig. 2) and tumor enrichment (Fig. 3). The concentration of **P$_{11\%}$** in the blood pool is lower compared to**P$_{7\%}$** but more effectively taken up by the tumor cells.

4. Conclusion

The present study clearly demonstrates that a controlled modification of HPMA–LMA block copolymers by means of PEGylation in the hydrophilic block has a tremendous impact on their pharmacokinetic profile *in vivo*. Radiolabeling of polymers with positron emitting isotopes such as fluorine-18 in combination with non-invasive positron emission tomography imaging enables to monitor their biodistribution pattern for up to 4 h with high spatial resolution in a quantitative way. This time span is too short to prove the EPR-effect. But it is perfectly suited to study, which parts of the body are reached as function of molecular structure and aggregate formation in aqueous solution. By means of these techniques, we observed that the degree of PEGylation of block copolymers was responsible for severe disparities in their biodistribution characteristics. Block copolymers with low amounts of PEG_{2000} side chains – exhibiting highest hydrodynamic radii – showed major kidney and MPS uptake. Blood retention as well as tumor accumulation was comparatively low. In contrast, higher PEG content caused prolonged blood circulation times of the HPMA based block copolymers and led even to a tumor accumulation constantly increasing with the amount of PEGylation. This observation supports the concept to selectively reduce the aggregate size of block copolymers by systematic PEG incorporation to fine-tune them for efficient anticancer therapy. Interestingly, **P$_{7\%}$** exhibited most favorable *in vivo* characteristics – including lowest hepatic and splenic uptake as well as highest blood pool concentration 4 h p.i. – but nevertheless **P$_{11\%}$** was the block copolymer with highest tumor accumulation in the Walker 256 mammary carcinoma over time.

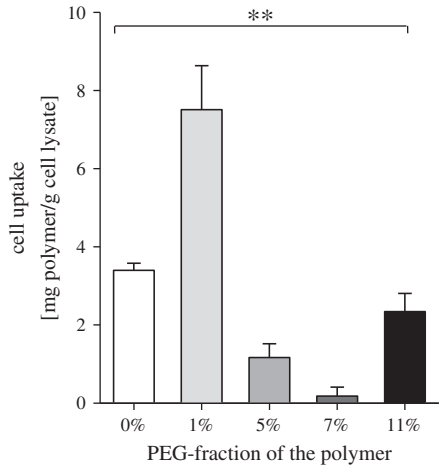

Fig. 6. Cellular uptake of the polymers after 2 h incubation at 37 °C in Walker 256 carcinoma cells *in vitro*; n = 6, (**) $p < 0.01$.

So there are general trends which can be understood but at the same time it is not possible to predict the exact fate of other, only slightly different polymers. One reason for the complexity of the amphiphilic block copolymers is the equilibrium between the large micellar aggregates (30 to 100 nm) and their constituent "unimers" (individual polymer chains). Both have to be considered concerning the interaction with the MPS, the basal membrane of the kidney and their cellular uptake — especially with regard to tumor cells. In our case the interaction with the MPS seems to be dominated by the size of the aggregates, while renal filtration is decided more on the level of the unimers. Tumor accumulation depended also on the "uptake-rate" of the tumor cells. In this "highly exploratory environment" it is the advantage of PET measurements to allow a "relatively" fast non-invasive screening of the body distribution and tumor accumulation of different polymers.

Acknowledgment

The authors would like to thank Barbara Biesalski, Nicole Bausbacher and Bengü Yilmaz for their support during animal studies and following interpretation. We also want to thank the Max-Planck Graduate Center (MPGC, M. Allmeroth) as well as the Graduate School Materials Science in Mainz (Excellence Initiative, DFG/GSC 266, D. Moderegger) for financial support. In addition the authors are very thankful for financial support of the DFG (Rösch: RO 985/30-1; Thews: TH 482/4-1; Zentel: ZE 230/21-1) and SAMT Initiative Mainz.

Appendix A. Supplementary data

Supplementary data to this article can be found online at http://dx.doi.org/10.1016/j.jconrel.2013.07.027.

References

[1] R. Duncan, The dawning era of polymer therapeutics, Nat. Rev. Drug Discov. 2 (5) (2003) 347–360.
[2] Y. Matsumura, H. Maeda, A new concept for macromolecular therapeutics in cancer chemotherapy: mechanism of tumoritropic accumulation of proteins and the antitumor agent smancs, Cancer Res. 46 (12 Part 1) (1986) 6387–6392.
[3] H. Maeda, J. Wu, T. Sawa, Y. Matsumura, K. Hori, Tumor vascular permeability and the EPR effect in macromolecular therapeutics: a review, J. Control. Release 65 (1–2) (2000) 271–284.

[4] A. Abuchowski, T. van Es, N.C. Palczuk, F.F. Davis, Alteration of immunological properties of bovine serum albumin by covalent attachment of polyethylene glycol, J. Biol. Chem. 252 (11) (1977) 3578–3581.

[5] R. Gref, A. Domb, P. Quellec, T. Blunk, R.H. Müller, J.M. Verbavatz, R. Langer, The controlled intravenous delivery of drugs using PEG-coated sterically stabilized nanospheres, Adv. Drug Deliv. Rev. 16 (2–3) (1995) 215–233.

[6] J.M. Harris, R.B. Chess, Effect of pegylation on pharmaceuticals, Nat. Rev. Drug Discov. 2 (3) (2003) 214–221.

[7] G. Pasut, F.M. Veronese, Polymer–drug conjugation, recent achievements and general strategies, Prog. Polym. Sci. 32 (8–9) (2007) 933–961.

[8] G. Pasut, F.M. Veronese, PEG conjugates in clinical development or use as anticancer agents: an overview, Adv. Drug Deliv. Rev. 61 (13) (2009) 1177–1188.

[9] M.J. Joralemon, S. McRae, T. Emrick, PEGylated polymers for medicine: from conjugation to self-assembled systems, Chem. Commun. 46 (9) (2010) 1377–1393.

[10] M.D. Howard, M. Jay, T.D. Dziubla, X. Lu, PEGylation of nanocarrier drug delivery systems: state of the art, J. Biomed. Nanotechnol. 4 (2) (2008) 133–148.

[11] A.S. Karakoti, S. Das, S. Thevuthasan, S. Seal, PEGylated inorganic nanoparticles, Angew. Chem. Int. Ed. 50 (9) (2011) 1980–1994.

[12] K. Ulbrich, V. Subr, Structural and chemical aspects of HPMA copolymers as drug carriers, Adv. Drug Deliv. Rev. 62 (2) (2010) 150–166.

[13] R. Duncan, L.W. Seymour, K.B. O'Hare, P.A. Flanagan, S. Wedge, I.C. Hume, K. Ulbrich, J. Strohalm, V. Subr, F. Spreafico, M. Grandi, M. Ripamonti, M. Farao, A. Suarato, Preclinical evaluation of polymer-bound doxorubicin, J. Control. Release 19 (1–3) (1992) 331–346.

[14] M.V. Pimm, A.C. Perkins, J. Strohalm, K. Ulbrich, R. Duncan, Gamma scintigraphy of the biodistribution of ^{123}I-labelled N-(2-hydroxypropyl)methacrylamide copolymer–doxorubicin conjugates in mice with transplanted melanoma and mammary carcinoma, J. Drug Target. 3 (5) (1996) 375–383.

[15] R. Duncan, Development of HPMA copolymer–anticancer conjugates: clinical experience and lessons learnt, Adv. Drug Deliv. Rev. 61 (13) (2009) 1131–1148.

[16] T. Lammers, V. Subr, K. Ulbrich, W.E. Hennink, G. Storm, F. Kiessling, Polymeric nanomedicines for image-guided drug delivery and tumor-targeted combination therapy, Nano Today 5 (3) (2010) 197–212.

[17] T. Minko, P. Kopecková, V. Pozharov, J. Kopecek, HPMA copolymer bound adriamycin overcomes MDR1 gene encoded resistance in a human ovarian carcinoma cell line, J. Control. Release 54 (2) (1998) 223–233.

[18] D.P. Nowotnik, E. Cvitkovic, ProLindac(TM) (AP5346): a review of the development of an HPMA DACH platinum polymer therapeutic, Adv. Drug Deliv. Rev. 61 (13) (2009) 1214–1219.

[19] M. Allmeroth, D. Moderegger, B. Biesalski, K. Koynov, F. Rösch, O. Thews, R. Zentel, Modifying the body distribution of HPMA-based copolymers by molecular weight and aggregate formation, Biomacromolecules 12 (7) (2011) 2841–2849.

[20] M. Hemmelmann, D. Kurzbach, K. Koynov, D. Hinderberger, R. Zentel, Aggregation behavior of amphiphilic p(HPMA)-co-p(LMA) copolymers studied by FCS and EPR spectroscopy, Biomacromolecules 13 (12) (2012) 4065–4074.

[21] G. Gaucher, M.-H. Dufresne, V.P. Sant, N. Kang, D. Maysinger, J.-C. Leroux, Block copolymer micelles: preparation, characterization and application in drug delivery, J. Control. Release 109 (1–3) (2005) 169–188.

[22] M. Barz, R. Luxenhofer, R. Zentel, A.V. Kabanov, The uptake of N-(2-hydroxypropyl)-methacrylamide based homo, random and block copolymers by human multi-drug resistant breast adenocarcinoma cells, Biomaterials 30 (29) (2009) 5682–5690.

[23] K. Kataoka, A. Harada, Y. Nagasaki, Block copolymer micelles for drug delivery: design, characterization and biological significance, Adv. Drug Deliv. Rev. 47 (1) (2001) 113–131.

[24] M. Talelli, C.J.F. Rijcken, C.F. van Nostrum, G. Storm, W.E. Hennink, Micelles based on HPMA copolymers, Adv. Drug Deliv. Rev. 62 (2) (2010) 231–239.

[25] K. Matyjaszewski, J. Xia, Atom transfer radical polymerization, Chem. Rev. 101 (9) (2001) 2921–2990.

[26] C.W. Scales, Y.A. Vasilieva, A.J. Convertine, A.B. Lowe, C.L. McCormick, Direct, controlled synthesis of the nonimmunogenic, hydrophilic polymer, poly(N-(2-hydroxypropyl) methacrylamide) *via* RAFT in aqueous media, Biomacromolecules 6 (4) (2005) 1846–1850.

[27] J. Chiefari, Y.K.B. Chong, F. Ercole, J. Krstina, J. Jeffery, T.P.T. Lee, R.T.A. Mayadunne, G.F. Meijs, C.L. Moad, G. Moad, E. Rizzardo, S.H. Thang, Living free-radical polymerization by reversible addition–fragmentation chain transfer: the RAFT process, Macromolecules 31 (1998) 5559–5562.

[28] E.R.G. Moad, S.H. Thang, Living radical polymerization by the RAFT process, Aust. J. Chem. 58 (2005) 379–410.

[29] M. Eberhardt, R. Mruk, R. Zentel, P. Théato, Synthesis of pentafluorophenyl(meth) acrylate polymers: new precursor polymers for the synthesis of multifunctional materials, Eur. Polymer J. 41 (7) (2005) 1569–1575.

[30] M.A. Gauthier, M.I. Gibson, H.-A. Klok, Synthesis of functional polymers by post-polymerization modification, Angew. Chem. Int. Ed. 48 (1) (2009) 48–58.

[31] M. Barz, M. Tarantola, K. Fischer, M. Schmidt, R. Luxenhofer, A. Janshoff, P. Theato, R. Zentel, From defined reactive diblock copolymers to functional HPMA-based self-assembled nanoaggregates, Biomacromolecules 9 (11) (2008) 3114–3118.

[32] M. Allmeroth, D. Moderegger, D. Gündel, K. Koynov, H.-G. Buchholz, K. Rausch, M. Schmidt, F. Rösch, R. Zentel, O. Thews, Impact of structure and size on body distribution but the individual tumor makes a difference: a quantitative *in vivo* PET study, Biomacromolecules (2013), http://dx.doi.org/10.1021/bm400709z, (submitted for publication).

[33] B. Hoang, H. Lee, R.M. Reilly, C. Allen, Noninvasive monitoring of the fate of ^{111}In-labeled block copolymer micelles by high resolution and high sensitivity microSPECT/CT imaging, Mol. Pharm. 6 (2) (2009) 581–592.

[34] Z.-R. Lu, Molecular imaging of HPMA copolymers: visualizing drug delivery in cell, mouse and man, Adv. Drug Deliv. Rev. 62 (2) (2010) 246–257.

[35] Y. Zhang, Y. Sun, X. Xu, X. Zhang, H. Zhu, L. Huang, Y. Qi, Y.-M. Shen, Synthesis, biodistribution, and microsingle photon emission computed tomography (SPECT) imaging study of technetium-99m labeled PEGylated dendrimer poly(amidoamine) (PAMAM)–folic acid conjugates, J. Med. Chem. 53 (8) (2010) 3262–3272.

[36] M. Kissel, P. Peschke, V. Subr, K. Ulbrich, A. Strunz, R. Kühnlein, J. Debus, E. Friedrich, Detection and cellular localisation of the synthetic soluble macromolecular drug carrier pHPMA, Eur. J. Nucl. Med. Mol. Imaging 29 (8) (2002) 1055–1062.

[37] Z. Yang, S. Zheng, W.J. Harrison, J. Harder, X. Wen, J.G. Gelovani, A. Qiao, C. Li, Long-circulating near-infrared fluorescence core-cross-linked polymeric micelles: synthesis, characterization, and dual nuclear/optical imaging, Biomacromolecules 8 (11) (2007) 3422–3428.

[38] H. Xie, Z.J. Wang, A. Bao, B. Goins, W.T. Phillips, *In vivo* PET imaging and biodistribution of radiolabeled gold nanoshells in rats with tumor xenografts, Int. J. Pharm. 395 (1–2) (2010) 324–330.

[39] G. Sun, A. Hagooly, J. Xu, A.M. Nyström, Z. Li, R. Rossin, D.A. Moore, K.L. Wooley, M.J. Welch, Facile, Efficient approach to accomplish tunable chemistries and variable biodistributions for shell cross-linked nanoparticles, Biomacromolecules 9 (7) (2008) 1997–2006.

[40] X. Sun, R. Rossin, J.L. Turner, M.L. Becker, M.J. Joralemon, M.J. Welch, K.L. Wooley, An assessment of the effects of shell cross-linked nanoparticle size, core composition, and surface PEGylation on *in vivo* biodistribution, Biomacromolecules 6 (5) (2005) 2541–2554.

[41] K.-I. Fukukawa, R. Rossin, A. Hagooly, E.D. Pressly, J.N. Hunt, B.W. Messmore, K.L. Wooley, M.J. Welch, C.J. Hawker, Synthesis and characterization of core-shell star copolymers for *in vivo* PET imaging applications, Biomacromolecules 9 (4) (2008) 1329–1339.

[42] M.M. Herth, M. Barz, M. Jahn, R. Zentel, F. Rösch, $^{72/74}$As-labeling of HPMA based polymers for long-term *in vivo* PET imaging, Bioorg. Med. Chem. Lett. 20 (18) (2010) 5454–5458.

[43] M.M. Herth, M. Barz, D. Moderegger, M. Allmeroth, M. Jahn, O. Thews, R. Zentel, F. Rösch, Radioactive labeling of defined HPMA-based polymeric structures using [18F] FETos for *in vivo* imaging by positron emission tomography, Biomacromolecules 10 (7) (2009) 1697–1703.

[44] C. Knoth, M. Hemmelmann, U. Schmitt, D. Moderegger, M. Allmeroth, M. Barz, C. Hiemke, K. Koynov, F. Rösch, R. Zentel, HPMA based amphiphilic copolymers mediate central nervous effects of domperidone, Macromol. Rapid Commun. 32 (9–10) (2011) 712–717.

[45] M. Hemmelmann, V.V. Metz, K. Koynov, K. Blank, R. Postina, R. Zentel, Amphiphilic HPMA–LMA copolymers increase the transport of Rhodamine 123 across a BBB model without harming its barrier integrity, J. Control. Release 163 (2) (2012) 170–177.

[46] P. Theato, Synthesis of well-defined polymeric activated esters, J. Polymer Sci., Part A: Polymer Chem. 46 (20) (2008) 6677–6687.

[47] S.b. Perrier, P. Takolpuckdee, C.A. Mars, Reversible addition–fragmentation chain transfer polymerization: end group modification for functionalized polymers and chain transfer agent recovery, Macromolecules 38 (6) (2005) 2033–2036.

[48] Hoffmann-La Roche AG, K. Conde-Knape, W. Danho, G. Ehrlich, N. Fotouhi, D.C. Fry, W. Khan, A. Konkar, C.M. Rondinone, J. Swistok, R.A. Taub, J.W. Tilley, Neuropeptide-2 receptor-agonists patent WO/2007/065808 (2007).

[49] P. Workman, E.O. Aboagye, F. Balkwill, A. Balmain, G. Bruder, D.J. Chaplin, J.A. Double, J. Everitt, D.A.H. Farningham, M.J. Glennie, L.R. Kelland, V. Robinson, I.J. Stratford, G.M. Tozer, S. Watson, S.R. Wedge, S.A. Eccles, Guidelines for the welfare and use of animals in cancer research, Br. J. Cancer 102 (11) (2010) 1555–1577.

[50] C. Konak, R.C. Rathi, P. Kopeckova, J. Kopecek, Effect of side-chains on solution properties of N-(2-hydroxypropyl)methacrylamide copolymers in aqueous solvents, Polymer 34 (22) (1993) 4767–4773.

[51] H. Hasse, H.P. Kany, R. Tintinger, G. Maurer, Osmotic virial coefficients of aqueous poly(ethylene glycol) from laser-light scattering and isopiestic measurements, Macromolecules 28 (10) (1995) 3540–3552.

[52] D.E. Owens Iii, N.A. Peppas, Opsonization, biodistribution, and pharmacokinetics of polymeric nanoparticles, Int. J. Pharm. 307 (1) (2006) 93–102.

[53] R. Gref, M. Lück, P. Quellec, M. Marchand, E. Dellacherie, S. Harnisch, T. Blunk, R.H. Müller, "Stealth" corona-core nanoparticles surface modified by polyethylene glycol (PEG): influences of the corona (PEG chain length and surface density) and of the core composition on phagocytic uptake and plasma protein adsorption, Colloids Surf. B: Biointerfaces 18 (3–4) (2000) 301–313.

[54] F. Alexis, E. Pridgen, L.K. Molnar, O.C. Farokhzad, Factors affecting the clearance and biodistribution of polymeric nanoparticles, Mol. Pharm. 5 (4) (2008) 505–515.

[55] M.R. Longmire, M. Ogawa, P.L. Choyke, H. Kobayashi, Biologically optimized nanosized molecules and particles: more than just size, Bioconjug. Chem. 22 (6) (2011) 993–1000.

[56] V.P. Torchilin, V.G. Omelyanenko, M.I. Papisov, A.A. Bogdanov Jr., V.S. Trubetskoy, J.N. Herron, C.A. Gentry, Poly(ethylene glycol) on the liposome surface: on the mechanism of polymer-coated liposome longevity, Biochim. Biophys. Acta Biomembr. 1195 (1) (1994) 11–20.